Transverse optical torque induced by localized surface plasmons

Ryoma Fukuhara, Yoshito Y. Tanaka, and Tsutomu Shimura

Transverse optical torque induced by localized surface plasmons

Ryoma Fukuhara,[1] Yoshito Y. Tanaka,[1, 2, *] and Tsutomu Shimura[1]

[1]*Institute of Industrial Science, University of Tokyo,*

4-6-1 Komaba, Meguro-ku, Tokyo 153-8505, Japan

[2]*Japan Science and Technology Agency, PRESTO,*

4-1-8 Honcho, Kawaguchi, Saitama 332-0012, Japan

(Dated: July 17, 2019)

Abstract

We report that localized surface plasmon resonance allows a single-element nanostructure to induce an extrinsic angular momentum of light in its interaction with a propagating plane wave. The recoil of the angular momentum results in an optical torque on the structure along an axis perpendicular to the optical axis, and the characteristics of this transverse torque depend on the incident polarization state, including the spin direction. Our results suggest that the designed dark plasmon mode can provide a new degree of freedom for optical manipulation of nanoparticles smaller than the diffraction limit.

* yoshito@iis.u-tokyo.ac.jp

I. INTRODUCTION

Light-matter interaction can induce a mechanical torque due to the transfer of angular momentum carried by light[1]. More than 70 years ago, Beth[2] first demonstrated that optical spin angular momenta (SAM) of a circularly polarized light can be transferred to materials. Then, Simpson et al. showed that orbital angular momenta (OAM) of a Laguerre-Gaussian laser mode are mechanically equivalent to SAM [3]. There have been a large number of studies on the application of optical torque manipulation for rotation of microparticles[4–7]. One of the main approaches involves the transfer of SAM to birefringent particles trapped by a focused laser beam with circular polarization[8]. However, this approach is unable to rotate particles for axes that are perpendicular to the optical axis, because the direction of SAM, which is intrinsic, is always along the direction of light propagation. Another approach is to utilize extrinsic angular momentum such as non-uniform irradiation to induce biased scattering force leading to an optical torque for the non-optical axis[9]. Thus, it is possible to nearly freely rotate particles larger than the light wavelength scale. This approach has been implemented in disparate fields such as microfluidics[9, 10] and biochemistry[11, 12].

However, the optical rotation for subwavelength-sized particles is still challenging because of the diffraction limit of light. It is obvious that the interaction between light and nanoparticles scales down for small interaction volumes, and this results in weaker optical torques than the effect of thermal fluctuations. Moreover, the diffraction limit restricts the freedom of the rotation axis. An approach similar to that used to rotate a microparticle about a non-optical axes is not available for nanoparticles smaller than the wavelength of the interacting light, because the particle in question experiences uniform light irradiation. One possible approach is to utilize intrinsic transverse angular momenta that are not parallel to the direction of propagation, that were recently discovered in some structural fields such as evanescent waves[13], surface plasmons[14], interference fields[15], or focused fields[16].

Localized surface plasmon resonance (LSPR) enhances the interaction between subwavelength-sized particles and light. In fact, studies on gold nanoparticle rotation that exploit plasmonic enhancement effects have been reported[17–19]. Furthermore, the plasmonic characteristics of nanoparticles strongly depend on their geometry. The nanostructures of various geometries have been reported with interesting optical properties such as negative refraction[20],

directional single photon sources[21], electromagnetically induced transparency[22], Fano resonances[23] and dark mode excitations[24]. Some geometries also allow to induce specific optomechanical responses, e.g. negative force[25] and lateral force[26]. Liu et al.[18] presented a nanostructure with phase retardation that can be rotated when illuminated with linearly polarized light, which has no angular momentum. This structure can transcribe its own phase pattern to the scattered light, which produces OAM and a recoil torque on the structure. Although LSPR introduces unconventional mechanical interaction, the rotation axis of manipulation was still restricted to the optical axis in previous studies, because the intrinsic angular momentum, such as SAM of circularly polarized light and OAM of vortex light was utilized.

In this report, we show an optical torque along an axis perpendicular to the optical axis for a single-element nanostructure with extrinsic angular momentum induced by LSPR. This torque is caused by the interaction between a simple plane wave and quadrupole components in plasmon modes based on the geometry of the structure. This interaction and the optical torque was realized with a V-shaped nanostructure, which has been widely used in the design of metasurfaces[27, 28]. Since the effective birefringence of the nanostructure has been previously discussed in detail, we have focused on the dark quadruple component based on the bent shape of the structure rather than on birefringence. There have been studies that the interaction between different plasmon modes, i.e. inter-mode interaction, of the V-shaped nanostructure leads to directional side scattering[29, 30]. It should be noted that the transverse torque discussed here is caused by the intra-mode interaction of individual V-shaped mode.

II. THEORY

The quadrupole can be considered as two coupled dipoles that are reversed with respect to each other. In the case of an isolated dipole, the imaginary part of the polarizability is generally positive, thereby satisfying the conservation law of energy. However, for a quadrupole, a negative imaginary part should be realized with one of the dipoles since the dipoles couple together and exchange energy. The two dipoles have a phase difference of π. Accordingly, one of the dipoles necessarily has a phase delay of π to 2π with respect to the incident electric field, which corresponds to the negative imaginary part of the polarizability

3

(and the dipole gives energy to the incident field).

Let us consider the optical force applied to the dipoles constituting the quadrupole. The directions of optical forces on dipoles with the phase difference of π would be inverse to each other. In other words, when one dipole experiences scattering and gradient forces in the direction of light propagation and a higher field intensity, the forces in the opposite direction must be exerted for the other dipole. The direction of the gradient force is reversed between the blue side and the red side from the resonant wavelength since the gradient force is proportional to the real part of the polarizability ($\boldsymbol{f}_{grad} = 1/2\mathrm{Re}\,\{\alpha\}\,\boldsymbol{\nabla}|E|^2$). However, the scattering force is proportional to the imaginary part of the polarizability, which determines the extinction of an incident wave ($\boldsymbol{f}_{scat} = \boldsymbol{k}/\epsilon\mathrm{Im}\,\{\alpha\} = \sigma_{ext}\boldsymbol{S}/c$), on the Rayleigh particle, where σ_{ext} and $\boldsymbol{S}$ are the extinction cross-section and the Poynting vector, respectively. Therefore, the direction of the scattering force on an isolated dipole is along the propagation of light, since the imaginary part is positive. However, considering the quadrupole as a combination of reversal dipoles, the imaginary part of the polarizability for one of the dipoles should be negative, and thus the scattering force on the dipole can be negative to the direction of propagation. This negative scattering force has gathered little attention because the net optical forces vanish on a whole quadrupole. Nevertheless, we focus on the optical torque generated by the reversal of the scattering forces.

The reversal of the optical forces on the dipoles in a plane orthogonal to the light propagation direction induces an optical torque along the y-axis perpendicular to the optical axis, as shown in Fig. 1. It should be noted that even a plane wave, which does not possess any angular momenta perpendicular to its propagation direction, could generate this transverse torque. Furthermore, the radiated field also does not have an angular momentum, considering the anti-symmetry of the quadrupole radiation. Thus, the transverse torque is due to the recoil of extrinsic angular momentum, which can be generated by the interference field between the incident field and the radiated field. However, in such a configuration as shown in Fig. 1, excitation of the quadrupole is difficult because of a mismatch of the symmetry between the uniform incident field and the quadrupole.

We considered such an interaction, followed by the transverse optical torque, to be realized by a single-element plasmonic nanostructure with a V-shaped geometry. The V-shaped nanostructure in Fig. 2a) has two orthogonal plasmon modes. Fig. 2b) shows the symmetric and antisymmetric mode excited by electric fields along the x-axis and y-axis, respectively.
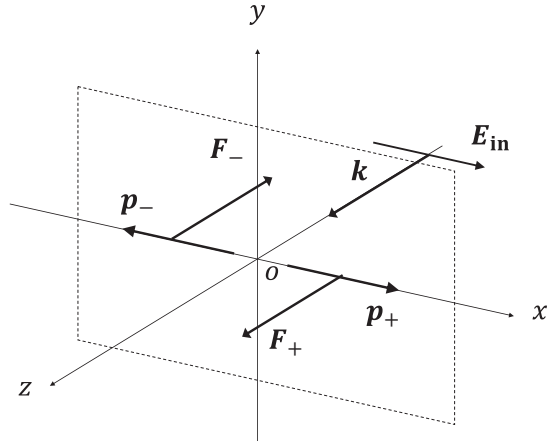
FIG. 1. Illustration of the coupled dipoles and the incident electric field. The signs of the dipoles and the incident field show their relative phase. The interaction between the incident electric field $\boldsymbol{E_{in}}$ with wave vector $\boldsymbol{k}$ and the coupled dipoles $\boldsymbol{p_\pm}$ can induce reversal forces $\boldsymbol{F_\pm}$, resulting in a transverse torque along the y-axis.

To analyze the optical force and torque on the nanostructure, we assumed a simple model for the V-shaped modes whereby they are represented as two coherent dipoles, $\boldsymbol{p_+}$ and $\boldsymbol{p_-}$, along the structure (Fig. 2c). An incident plane wave with arbitrary polarization in the xy-plane propagates along the z-axis. The symmetric and anti-symmetric modes are individually excited depending on the incident wavelength, as shown in Fig. 2b. The $\boldsymbol{p_+}$ and $\boldsymbol{p_-}$ of the symmetric mode can be expressed as:

$$\boldsymbol{p_\pm} = \pm\alpha_S E_y \boldsymbol{e_{\pm\theta}} \tag{1}$$

where $\boldsymbol{e_{\pm\theta}}$ are unit vectors with an angle of $\pm\theta$ relative to the x-axis, and $\alpha_S = \alpha'_S + i\alpha''_S$ represents the polarizability of the symmetric mode. The symmetric mode is excited by the y-component E_y of the incident field, but $\boldsymbol{e_{\pm\theta}}$ have both x and y-components. This mode consists of not only a dipole moment parallel to its excitation polarization, but also a local polarization along the x-axis. Since the x components of $\boldsymbol{p_\pm}$ are coherent and inverse to each other, they have quadrupole-like behavior, although the x components are canceled. When the incident field has its x-component as well as E_y to excite the symmetric mode, the configuration of the coupled two dipoles and the incident field in Fig. 1 can be realized. It should be noted that the x-component of the incident field does not excite any plasmon modes, that is, no energy exchange occurs between the incident light and the structure. In

5

addition, since the polarization directions to excite the dipoles and to interact with them in Fig. 1 are orthogonal, their relative phase can control the directions of the optical forces and the transverse torque.

Substituting eq.(1) into the optical force expression;

$$\boldsymbol{f} = \sum_{j=x,y,z} \frac{1}{2}\mathrm{Re}\left[p_j^* \cdot \boldsymbol{\nabla}E_j\right] \tag{2}$$

we obtain the optical force along the z-axis exerted on $\boldsymbol{p}_+$ and $\boldsymbol{p}_-$;

$$
\begin{aligned}
f_{\pm,z} = &\frac{1}{2}\alpha_S' \sin\theta\,\mathrm{Re}\left[E_y^*\frac{\partial E_y}{\partial z}\right] + \frac{1}{2}\alpha_S'' \sin\theta\,\mathrm{Im}\left[E_y^*\frac{\partial E_y}{\partial z}\right] \\
&\pm\frac{1}{2}\mathrm{Re}\left[\alpha_S \cos\theta E_y^*\frac{\partial E_x}{\partial z}\right]
\end{aligned}
\tag{3}
$$

The first and second term represents the conventional optical gradient force and the scattering force, respectively, through the interaction between E_y and the dipole moments along the y-axis. The last term of this model represents the interaction between E_x and the quadrupole-like component excited by E_y. The transverse optical torque along the y-axis can be obtained by $N_y = -l/2\cos\theta(f_{+,z} - f_{-,z})$, where the signs of the term between f_+ and f_- are opposite to each other. In other words, the quadrupole-like component on the bent shape of the structure results in the transverse torque. The contribution from the anti-symmetric mode is also calculated similarly. Thus, we obtain the total torque on the nanostructure, which is the simple sum of the contributions from the two modes;

$$
\begin{aligned}
N_y = -\frac{l}{2}\cos\theta\Bigg\{&\cos\theta\left(\alpha_S'\mathrm{Re}\left[E_y^*\frac{\partial E_x}{\partial z}\right] + \alpha_S''\mathrm{Im}\left[E_y^*\frac{\partial E_x}{\partial z}\right]\right) \\
&+\sin\theta\left(\alpha_A'\mathrm{Re}\left[E_x^*\frac{\partial E_y}{\partial z}\right] + \alpha_A''\mathrm{Im}\left[E_x^*\frac{\partial E_y}{\partial z}\right]\right)\Bigg\}
\end{aligned}
\tag{4}
$$

III.   NUMERICAL ANALYSIS

In order to obtain physical insight into the transverse torque, we show the wavelength dependence of the torque for linear and circular incident polarizations in Fig. 3. The polarizabilities α_S and α_A in Eq. 3 are obtained from an electromagnetic simulation using the finite element method as following. The dipole moment p of right arm $(x > 0)$ is calculated by the integration of the polarization along the arm direction for the right-half
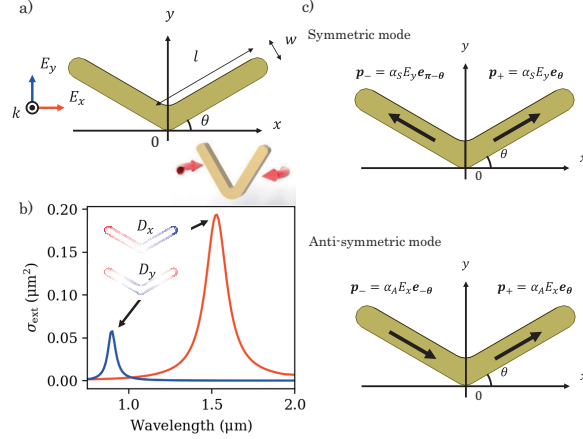
FIG. 2. a) Geometry of the analysis. The material of the V-shaped structure and surrounding is gold and SiO_2, respectively. The inset shows an illustration of the transverse optical torque on the nanostructure. b) The resonant spectra of the plasmonic modes for the condition $l = 120\,\text{nm}$, $w = 40\,\text{nm}$, $\theta = 30°$ and the thickness of $30\,\text{nm}$. The blue and orange lines indicate the extinction in the case of an incident electric field with x and y-polarization states, respectively. The insets show the typical charge density distribution of the symmetric mode D_y and the anti-symmetric mode D_x. c) Schematics of the model analysis for each mode, where α_S and α_A represent the polarizability of the symmetric and anti-symmetric modes, respectively, and e_θ represents a unit vector angled relative to the x-axis. The incident field is assumed to be a plane wave propagating along the z-axis with arbitrary polarization in the xy-plane.

domain D of V-structure as $p = \int_D P \cdot e_\theta$, where e_θ is the unit vector along the arm with angle θ (which is similar approach to Refs. [29, 30]). The dipole moments yield to the polarizabilities α_S and α_A for the incident electric field along the y and x axis, respectively, as $\alpha = p/E_0$, where E_0 is the complex amplitude of the incident electric field at the $z = 0$ plane. The torques calculated based on our simple model are in good agreement with those calculated rigorously from the conservation law of angular momentum using Maxwells stress tensor[1].

For the incident linear polarization $\boldsymbol{E} = E_0 \begin{pmatrix} \cos\phi \\ \sin\phi \end{pmatrix} e^{i(kz-\omega t)}$, the transverse torque is represented by:

$$N_y = -\pi l I_0 Z_0 \mu_r \cos\theta \sin 2\phi \frac{\alpha_S'' \cos\theta + \alpha_A'' \sin\theta}{\lambda} \tag{5}$$

7
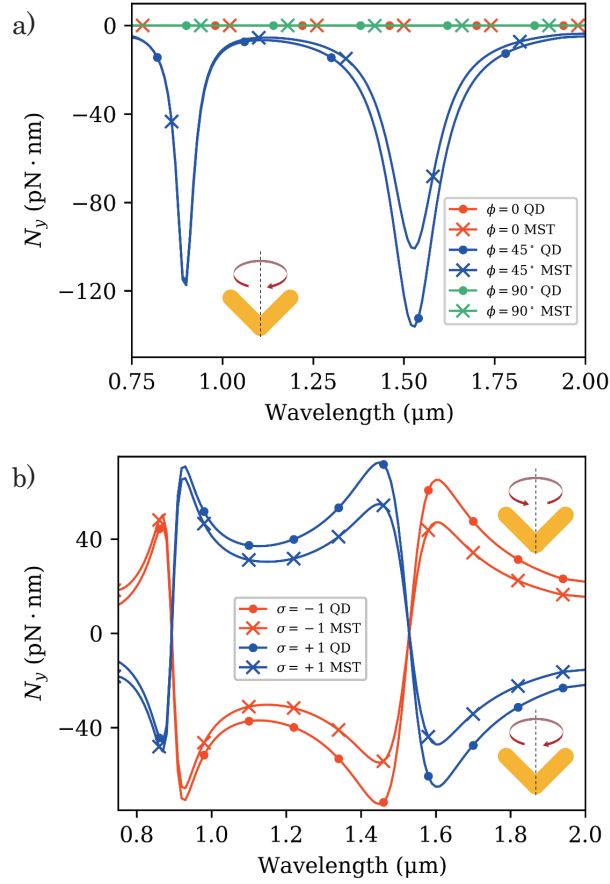
FIG. 3. Optical torque along y-axis for the V-shaped structure in Fig.2 versus the incident wavelength in the case of linear polarization a) and circular polarization b). The torque is normalized with the incident intensity $(10\,\mathrm{mW}/\mu\mathrm{m}^2)$. The dot marks and cross marks represent the results of the coupled dipoles model analysis and the Maxwell stress tensor calculation. The insets indicate the directions of the torques. (a) The colors orange, blue and green correspond to $0°$, $45°$ and $90°$ respectively of the incident polarization angle. The torque can be generated only for the incident electric field with both x and y-components. (b) The colors orange and blue corresponds to left and right circular polarization, respectively. The sign of the torque depends on the left or right polarization of the incident field.

where I_0 is the incident field intensity, Z_0 is the impedance in a vacuum, and μ_r is the permeability. Fig. 3(a) shows that no torque can be generated for only x or y-polarization, which indicates that both polarization components are essential to realize the configuration of the coupled two dipoles and the incident field in Fig. 1. The peak wavelengths of the torque

8

correspond to the plasmon resonance peaks of the symmetric and anti-symmetric modes in Fig. 2(b), i.e. the imaginary parts of the polarizability. The difference of the torque magnitudes in the longer wavelength region between the coupled dipoles model analysis and the Maxwell stress tensor calculation can be explained by the property of the anti-symmetric mode, which is geometrically biased toward the center of the structure.

For the incident circular polarization $\boldsymbol{E} = E_0 \begin{pmatrix} 1/\sqrt{2} \\ i\sigma/\sqrt{2} \end{pmatrix} e^{i(kz-\omega t)}$, the torque is represented by:

$$N_y = \sigma \pi l I_0 Z_0 \mu_r \cos\theta \frac{\alpha'_S \cos\theta - \alpha'_A \sin\theta}{\lambda} \tag{6}$$

where $\sigma = -1, +1$ is spin direction corresponding to $\sigma^{\pm}$ circular polarization. Fig. 3(b) shows that the direction of the torque depends on the incident spin direction because the relative phase in Fig. 1 has the difference of π between $\sigma^{\pm}$ circular polarizations. Unlike the case of the linear polarization, the torque for the circular polarization changes between positive and negative values at the resonance peaks, which reflect its dependence on the real part of the polarizability. Thus, the incident polarization state determines whether the torque is proportional to the imaginary part or the real part of the polarizability. This is attributed to the mechanism of the torque generation that requires a phase difference of $\pi/2$ between the coupled dipoles and the interacting component of the incident field. For linearly polarized field, the coupled dipoles and the interacting field are in phase, resulting in a dependence on the imaginary part. In contrast, for the circularly polarized field, the optical torque depends on the real part of the polarizability, because the phase of the coupled dipoles is shifted by $\pi/2$ from that of the interacting field.

To understand the plasmon modes of the V-shaped nanostructure generating the transverse optical torque, we considered simple two nanorods arranged in a V-shape, which can be analytically solved by the discrete dipole approximation as two dipoles with the interaction through their dipole radiation (details in Appendix). When two nanorods are separated by about the resonant wavelength of an isolated nanorod, their dipoles separately oscillate and the imaginary parts of their polarizabilities are always positive because of their weak interaction. As they are closer than the wavelength, the inherent plasmon modes of the nanorods hybridize into two new modes through strong interaction and coupling. One of the new modes has a shorter resonant wavelength and excited by the y-polarized incident field. The other has a longer wavelength and excited by the x-polarized field. The former and the lat-

ter correspond to the symmetric and anti-symmetric modes of the V-shaped nanostructure, respectively, (which are considered as the hybridized modes in the strong-coupling limit). In other words, the hybridization results in the transverse optical torque.

In general, the bent-shape nanostructures that are not point-symmetric but line-symmetric with respect to the torque axis can induce the transverse torques in the same manner of the V shape. In addition, asymmetric structures allow the direct excitation of the quadrupole mode in a plane orthogonal to the incident light direction, resulting in the transverse torque. The torque magnitude on these structures changes with their rotation. Here, we consider the effect of the change of the V structure orientation on the optical torque $N = r \times F$. The main effects would be the following three points. a) Decrease of the excitation efficiency of the symmetric and anti-symmetric modes due to the angle deviations $\Delta\phi_x$ around the x-axis and $\Delta\phi_y$ around the y-axis, respectively, in the coordinates illustrated in Fig. 2, i.e. $F_{sym} \propto \cos\Delta\phi_x$, $F_{anti-sym} \propto \cos\Delta\phi_y$. b) Decrease of the separation d_x between the two out-of-phase dipole components due to the angle deviation $\Delta\theta_x$, i.e. $r = d_x/2 \propto \cos\Delta\phi_y$. c) Phase retardation of the incident electric fields on the two out-of-phase dipole components with the separation d_z due to the angle deviation $\Delta\theta_y$, i.e. $kd_z \propto k\sin\Delta\phi_y$, where k is the wavenumber of the incident light. These effects change the magnitude of the optical torque as it rotates the V structure. The nanostructures that are three-dimensionally line-symmetric with the torque axis would allow the constant torque over the rotation. Three-dimensional line-symmetric or asymmetric nanostructures would allow the constant torque over the rotation.

One of the possible applications of the plasmonic structures, which have specific optomechanical responses, would be light-driven nanoactuators that could autonomously operate without predetermined angular momentum of the illumination light (instead, the momentum acquired from the designed plasmonic structure). In such applications, the nanostructures is mounted on larger structures, which can reduce the Brownian random motion, as demonstrated in the experimental work [18]. To show the feasibility, we compared our optical torque to Brownian motion torque $N_B = \sqrt{2\gamma k_B T} \sim 14\text{pN}\cdot\text{nm}$ in the typical case of the nanostructure mounted in the sphere with the radius of $1\,\mu$m, floating in water. The damping coefficient is calculated as $\gamma = 8\pi\mu a^3$, where a is the radius of the sphere, and μ is the viscosity of water[31]. Fig.3 indicates that an intensity of $10\,\text{mW}/\mu\text{m}^2$ would be enough to control the rotation of the microsphere under thermal fluctuations.

IV. CONCLUSION

In summary, we have shown that a single-element V-shaped nanostructure under normal plane wave illumination experiences an optical torque along a symmetric axis perpendicular to the optical axis, due to the extrinsic angular momentum induced by LSPR, using model analysis and electromagnetic simulation. This transverse torque strongly depends on not only the wavelength but also the polarization state, including the spin direction of the illumination light. We revealed that the extraordinary torque is due to the recoil of the extrinsic angular momentum caused by the interaction between the propagating plane wave and the dark quadrupole component in plasmon modes, based on the geometry of the structure. This suggests Such plasmonic structures could be applied for light-driven nanoactuators that autonomously operate without predetermined incident light momentum. If some nanoactuators with different resonances and functions are accumulated even within the area smaller than the diffraction limit, their specific function could be addressed with the illumination light wavelength. Moreover, we suggest that the optical torque or angular momentum reflects the local change of the electromagnetic field which is negligible in the far-field optical response, and that the measurement of this parameter could facilitate a new method to characterize the physical properties of nanoparticles, which is difficult with other spectroscopy-based techniques. Additionally, the transverse optical torque consists of a reverse optical scattering force including one that is negative to the direction of light propagation. In recent years, the negative scattering force has attracted much attention and has been studied using various approaches such as with a gain medium and using a Bessel beam[32, 33]. Our study can also be considered as one that realizes and utilize the negative scattering force from LSPR.

Appendix: Discrete dipole approximation (DDA)

In order to analytically solve the two-dipole model by the discrete dipole approximation (DDA), we consider simple two nanorods arranged in a V-shape (Fig.4), which can be approximated as two dipoles with the interaction through their dipole radiation

$$\boldsymbol{E}_{rad}(\boldsymbol{r}, \boldsymbol{p}) = \frac{1}{4\pi\epsilon} \left\{ \frac{\omega^2}{c^2 r} \left[(\boldsymbol{e_r} \times \boldsymbol{p}) \times \boldsymbol{e_r} \right] + \frac{1}{r^2} \left(1 - \frac{i\omega}{c} \right) \left[3\boldsymbol{e_r}(\boldsymbol{e_r} \cdot \boldsymbol{p}) - \boldsymbol{p} \right] \right\} e^{ikr}, \qquad (A.1)$$
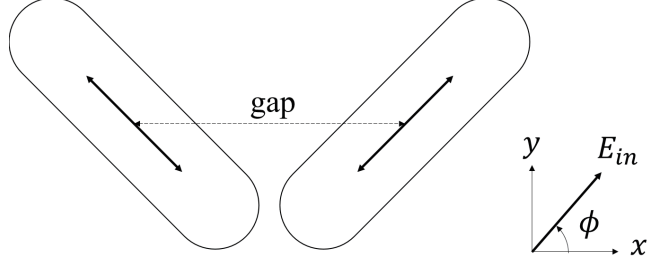
FIG. 4. Schematic illustration of the DDA model

where $r = |\boldsymbol{r} - \boldsymbol{r}_d|$, $\boldsymbol{e_r} = (\boldsymbol{r} - \boldsymbol{r}_d)/|\boldsymbol{r} - \boldsymbol{r}_d|$, and $\boldsymbol{p}$ and $\boldsymbol{r}_d$ correspond to the dipole moment and position of the radiating dipole. The electric fields at the left and right dipoles are sum of the incident electric field and radiated field from each other. Therefore, following self-consistent equations are obtained

$$\boldsymbol{E}_1 = \boldsymbol{E}_{in} + \boldsymbol{E}_{rad}(\boldsymbol{r}_1, \boldsymbol{p}_2) \tag{A.2}$$

$$\boldsymbol{E}_2 = \boldsymbol{E}_{in} + \boldsymbol{E}_{rad}(\boldsymbol{r}_2, \boldsymbol{p}_1) \tag{A.3}$$

$$\boldsymbol{p}_1 = \bar{\alpha}_1 \boldsymbol{E}_1 \tag{A.4}$$

$$\boldsymbol{p}_2 = \bar{\alpha}_2 \boldsymbol{E}_2, \tag{A.5}$$

where $\bar{\alpha}_{1,2} = \alpha \boldsymbol{e}_{1,2} \boldsymbol{e}_{1,2}^T$ are the polarizability tensors of each dipole, α is the longitudinal polarizability of a single nanorod, and $\boldsymbol{e}_{1,2}$ are the unit vectors along each dipole. We obtained $\boldsymbol{p}_1, \boldsymbol{p}_2$ by solving these equations for electric field. The polarizabilities of individual dipoles are obtained from FEM simulation (p0 in Fig. 5) and these have a birefringence inherited from the nanorods. Fig. 5 show the results of DDA calculation. When the two dipoles are separated by about the resonance wavelength of an isolated dipole, their dipoles separately oscillate according to the inherent polarizabilities, and the imaginary parts of their polarizabilities are always positive because of their weak interaction. As they are closer than the wavelength, the inherent plasmon modes of the dipoles hybridize into two new modes through strong interaction and coupling. One of the new modes has a shorter resonant wavelength and excited by the y-polarized incident field, and the oscillation of the dipoles are in phase along the y direction. The other has a longer resonant wavelength and excited by the x-polarized incident field, and the oscillation of the dipoles are in phase along the x direction. The former and latter correspond to the symmetric mode and the anti-symmetric mode for a V-shaped nanostructure, respectively. In other words, the hybridization results in the

12
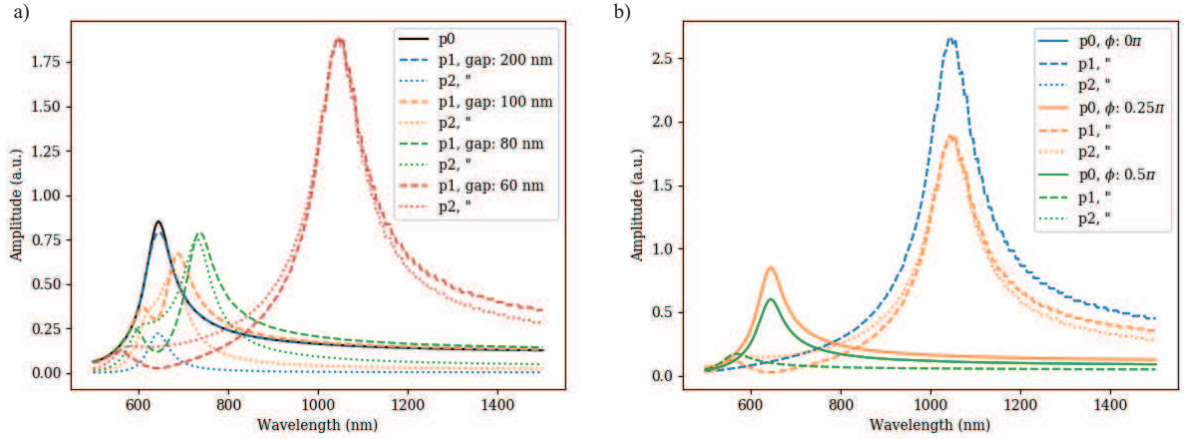
FIG. 5. Results of DDA calculation. a) The gap dependence of the amplitudes of dipole moments $|\boldsymbol{p}|$ versus the wavelength of the incident linear polarized light with polarization angle: $\varphi = 45°$. Black line represents the result for an isolated dipole. Colored lines represent the results for the two dipole moments gapped by 200, 100, 80 and 60 nm. b) The polarization angle dependence of the amplitudes of dipole moments with gap of 60 nm versus the wavelength of the incident linear polarized light. Colored lines represent the results for the polarization angle of 0, $\pi/4$, $\pi/2$.

configuration of the coupled two dipoles and the incident field along the axis perpendicular to the excitation polarization direction, as shown in Fig. 1. Consequently, the imaginary part of one of these coupled dipole moments becomes negative.

[1] P. H. Jones, O. M. Maragó, and G. Volpe, Optical Tweezers: Principles and Applications (Cambridge University Press, 2015).

[2] R. A. Beth, Phys. Rev. **50**, 115 (1936).

[3] N. B. Simpson, K. Dholakia, L. Allen, and M. J. Padgett, Opt. Lett. **22**, 52 (1997).

[4] S. Sato, M. Ishigure, and H. Inaba, Electron. Lett. **27**, 1831 (1991).

[5] E. Higurashi, R. Sawada, and T. Ito, Phys. Rev. E. **59**, 3676 (1999).

[6] L. Paterson, M. P. MacDonald, J. Arlt, W. Sibbett, and et al, Science **292**, 912 (2001).

[7] A. T. O'Neil and M. J. Padgett, Opt. Lett. **27**, 743 (2002).

[8] A. I. Bishop, T. A. Nieminen, N. R. Heckenberg, and H. Rubinsztein-Dunlop, Phys. Rev. Lett. **92**, 198104 (2004).

[9] T. Asavei, T. A. Nieminen, V. L. Y. Loke, A. B. Stilgoe, R. Bowman, D. Preece, M. J. Padgett, N. R. Heckenberg, and H. Rubinsztein-Dunlop, New J. Phys. **15**, 063016 (2013).

[10] J. Leach, H. Mushfique, R. di Leonardo, M. Padgett, and J. Cooper, Lab Chip **6**, 735 (2006).

[11] H. Florian, W. Mike, M. Stephanie, M. Berenike, and D. Cornelia, J. Biophoton. **3**, 468 (2010).

[12] M. K. Kreysing, T. Kießling, A. Fritsch, C. Dietrich, J. R. Guck, and J. A. Käs, Opt. Express **16**, 16984 (2008).

[13] K. Y. Bliokh, A. Y. Bekshaev, and F. Nori, Nat. Commun. **5**, 3300 (2014).

[14] Q. Zhang, J. Li, X. Liu, D. J. Gelmecha, and W. Zhang, Phys. Rev. A **97**, 013822 (2018).

[15] A. Y. Bekshaev, K. Y. Bliokh, and F. Nori, Phys. Rev. X **5**, 011039 (2015).

[16] K. Y. Bliokh, F. J. Rodriguez-Fortuno, F. Nori, and A. V. Zayats, Nat. Photonics **9**, 796 (2015).

[17] A. Lehmuskero, R. Ogier, T. Gschneidtner, P. Johansson, and M. Käll, Nano Lett. **13**, 3129 (2013).

[18] M. Liu, T. Zentgraf, Y. Liu, G. Bartal, and X. Zhang, Nature Nanotech. **5**, 570 (2010).

[19] L. Shao, Z.-J. Yang, D. Andrén, P. Johansson, and M. Käll, ACS Nano **9**, 12542 (2015).

[20] R. A. Shelby, D. R. Smith, and S. Schultz, Science **292**, 77 (2001).

[21] A. G. Curto, G. Volpe, T. H. Taminiau, M. P. Kreuzer, R. Quidant, and N. F. van Hulst, Science **329**, 930 (2010).

[22] S. Zhang, D. A. Genov, Y. Wang, M. Liu, and X. Zhang, Phys. Rev. Lett. **101**, 047401 (2008).

[23] B. Luk'yanchuk, N. I. Zheludev, S. A. Maier, N. J. Halas, P. Nordlander, H. Giessen, and C. T. Chong, Nature Mater. **9**, 707 (2010).

[24] R. M. Kerber, J. M. Fitzgerald, D. E. Reiter, S. S. Oh, and O. Hess, ACS Photonics **4**, 891 (2017).

[25] H. Liu, J. Ng, S. B. Wang, Z. F. Lin, Z. H. Hang, C. T. Chan, and S. N. Zhu, Phys. Rev. Lett. **106**, 087401 (2011).

[26] S. B. Wang and C. T. Chan, Nat. Commun. **5**, 3307 (2014).

[27] N. Yu, F. Aieta, P. Genevet, M. A. Kats, Z. Gaburro, and F. Capasso, Nano Lett. **12**, 6328 (2012).

[28] N. Yu, P. Genevet, M. A. Kats, F. Aieta, J.-P. Tetienne, F. Capasso, and Z. Gaburro, Science **334**, 333 (2011).

[29] D. Vercruysse, Y. Sonnefraud, N. Verellen, F. B. Fuchs, G. D. Martino, L. Lagae, V. V. Moshchalkov, S. A. Maier, and P. V. Dorpe, Nano Lett. **13**, 3843 (2013).

[30] D. Vercruysse, X. Zheng, Y. Sonnefraud, N. Verellen, G. D. Martino, L. Lagae, G. A. E. Vandenbosch, V. V. Moshchalkov, S. A. Maier, and P. V. Dorpe, ACS Nano **8**, 8232 (2014).

[31] L. D. Landau and E. M. Lifshitz, Fluid Mechanics: Volume 6 (Course of Theoretical Physics), 2nd ed. (Pergamon, Oxford, 2013).

[32] O. Brzobohatý, V. Karásek, M. Šiler, L. Chvátal, T. Čižmár, and P. Zemánek, Nat. Photonics **7**, 123 (2013).

[33] A. Dogariu, S. Sukhov, and J. Sáenz, Nat. Photonics **7**, 24 (2012).